Journal of Biotechnology & Biomaterials

Kristin Sundberg et al., J Biotechnol Biomater
2020, 10:4

Research Article Open Access

Microstructural Characterization of Conventional and Nanomaterial Copper Cold Spray Coatings

Kristin Sundberg*, Caitlin Walde, Bryer Sousa, Swetaparna Mohanty, Jae-Hwang Lee, Victor Champagne, Richard Sisson and Danielle Cote

Army Research Labs, Worcester Polytechnic Institute, Massachusetts, United States

Abstract

The microstructure of conventional and nanomaterial Cu cold spray coatings is explored to understand why nanomaterial Cu cold spray performs better than conventional Cu cold spray in the contact killing of Influenza A virus. Powder, single-splats from laser induced projectile impact testing (LIPIT), and consolidated cold spray coatings are imaged using Scanning Electronmicroscopy (SEM). Sample composition is confirmed using Energy Dispersive X-Ray Spectroscopy (EDS) and X-ray Diffraction (XRD). Results show nanomaterial Cu to have a much smaller grain size than conventional Cu. Nanoindentation is used to confirm microstructural differences, showing nanomaterial Cu to have greater hardness. LIPIT and consolidated cross-sections identified grain refinement at the particle-substrate interface for both nanomaterial and conventional Cu. Follow-on work with corrosion testing will be performed to better understand Cu ion release rate in relation to the differing material microstructures for antimicrobial applications.

Keywords: Cold spray; Nanomaterial; Copper; Antimicrobial; Grain refinement; Work hardening

Introduction

Microstructural characterization of conventional and nanomaterial Cu coatings is done in support of prior work in the paper, "Effectiveness of Nanomaterial Copper Cold Spray Surfaces on Inactivation of Influenza a Virus", where it was found that nanomaterial Cu had greater antimicrobial effectiveness than conventional Cu [1]. Understanding microstructural changes in powder, single-splat, and consolidated Cu cold spray will help to better determine Cu kill mechanisms and to further optimize Cu antimicrobial properties for future coatings.

Cold spray coatings have a distinct bonding at the particle/substrate interface, which contributes to its strong adhesive properties [2]. For a strong bond to occur in a single-splat, the particle impact velocity must exceed a critical value and the particle cooling rate should be low enough for shear instability/localized deformation, but also high enough for cooling of the bond to occur [13,4]. Factors affecting this include the material, powder quality, size, shape, impact temperature, and velocity [5]. One of the reasons why nano-agglomerate copper powder is used instead of nano particles is because nano particle diameters are too small for shear instabilities as their thermal gradient/cooling rate is too high [6]. For copper cold spray, the critical diameter, or minimum diameter for particle/substrate adhesion is 10 um's [16]. For this work, the average particle size of conventional and nano-agglomerate Cu powder is -31/+5 and 25 um's, respectively [6].

The critical impact velocity (Vc) for a given particle size can be predicted using modelling techniques [7]. or with trial and error, as is the case of the Laser Induced Projectile Impact Testing (LIPIT) performed in this paper. LIPIT is able to impact individual powder particles on a substrate at varying velocities to determine the ideal velocity for increased adhesion and reduced particle rebounding (Figure 1). LIPIT can provide information on impact mechanics, showing the strong dependence of compressive shock on the characteristic cold spray 'mixing' at the interface and 'jetting' at the particle-substrate surface [MIT].

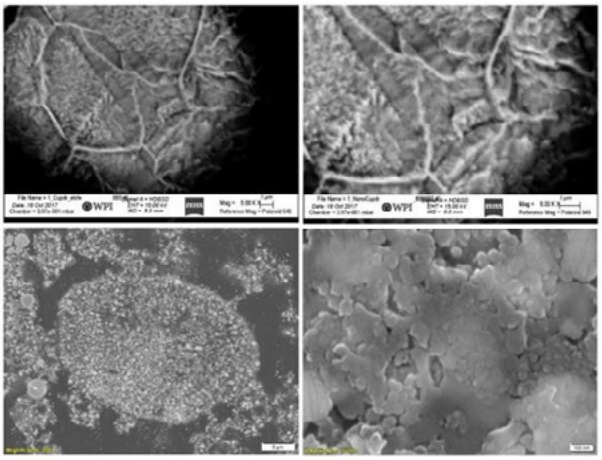

Figure 1: SEM backscatter micrographs of etched conventional Cu powder particle (top). FE SEM micrographs of etched nano-agglomerate Cu powder (bottom).

Due to the relatively low temperatures of cold spray (100-600oC), a high impact velocity (600-1000 m/s) is needed for good adhesion. This increase in velocity results in high plastic deformation which can cause dynamic recrystallization, producing ultra-fine-grain (UFG) structures at particle-particle and particle-substrate interfaces. Dynamic recrystallization occurs from high shear due to plastic deformation or from mechanical stress where rotational dynamic recrystallizationmay occur.

***Corresponding author:** Kristin Sundberg, Army Research Labs, Worcester Polytechnic Institute, Massachusetts, United States, E-mail: kristinsundberg7@yahoo.com

Received date: 24-02-2020; **Accepted date:** 09-03-2020; **Published date:** 16-03-2020

Material properties can affect UFG development through recrystallization, where a decrease in thermal conductivity increases heat retention, increasing the potential for recrystallization [5,8-11].

Upon impact, interface mixing is dependent on substrate and powder hardness and density. A hard metal impacting a softer metal would have a deeper imprint with less spreading than a soft metal on a hard substrate. In the case of Cu and Al, both are soft metals, with Cu having slightly higher density. The depth of impact is amplified by the copper particle being heavier and having a larger amount of kinetic energy than that of the Al substrate. Also, soft metals have a greater temperature region from high ductility and thermal softening, which contributes to the spreading of the particle on impact [2,4].

The same characteristic mixing discussed above applies to cold sprayed nanomaterial Cu coatings [6]. In some cases, nano-particles can have partial devitrification of their amorphous phase, but inmost cases the nano structure is retained [5].

Cold spray is known to have very few oxides/impurities/inclusions in the bulk coating; this is due to the quality of the powder, but also to the peening effect. When the particles are sprayed, the impact against the substrate breaks up oxides, which are then carried up the surface with the interfacial jet [4]. Work with EDS and XRD can confirm powder and coating purity (Figure 2).

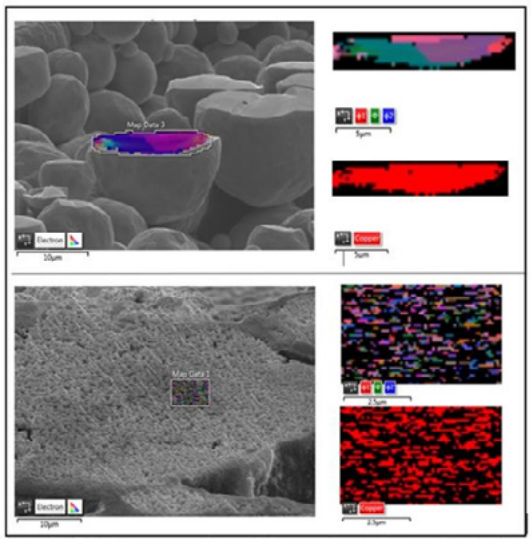

Figure 2: EBSD cross-sections of Conventional Cu powder (top) and Nanomaterial Cu powder (bottom).

Hardness measurement can be used to predict cold spray microstructural properties in powder and consolidated coating using the Hall-Petch relationship, which states that grain-boundary strengthening, and subsequent material yield strength, increases with decreasing grain size [12]. Hall-Petch is commonly used in the micrometer range but has also been demonstrated for nanocrystalline metals ranging 20-100 nm [13]. It appears that the relation holds true for consolidated nanomaterial Cu cold spray, which has much greater hardness values and much smaller grains than that of conventional Cu cold spray [6]. There is a direct relationship between Cumaterial hardness and antimicrobial properties [6]. The effect of microstructure on end material properties is key in understanding why nanomaterial Cu is more effective at contact killing of Influenza A virus than conventional Cu.

μ-Projectile and target substrate preparation

PDMS (Sylgard 184, Dow Chemical) with a mixing weight ratio of 1:10 was spin coated onto an ~80 nm thick Au coated glass substrate (Fisherbrand TM Cover Glasses No. 2) [6]. They were further cured at 200°C for 1 hr. Nano-agglomerate Cu powder and conventional Cu powder with particle diameter of approximately 15-20 μm were used for the experiments. The particles were applied to the surface of the PDMS/Au coated glass substrate using a brush. High purity Al target substrates (5 mm x 5 mm) were electropolished and used for the experiments. The electrolyte solution used was a mixture of Perchloric acid (70% Perchloric acid Sigma-Aldrich) and Ethanol (Sigma-Aldrich) in volume ratio of 1:5. During the process, the electrolyte bath temperature range was maintained in between 5°C to 8°C and the electropolishing was carried out at 15 V for a duration of 10 minutes.

High strain rate single particle experiments

Acceleration of the micron scale particles to supersonic velocities was achieved by using Laser-induced projectile impact test (LIPIT) technique [14,15]. Briefly described, a Nd:YAG laser (Quanta-Ray INDI-40-10-HG, Spectra-Physics) was used to create an ablation laser pulse (5-8 n s pulse duration; 1064 nm) [14]. Following the laser ablation of the Au film after trigger, the PDMS film expands and the selected particle that was positioned at the focus point of the ablation laser accelerates towards the target (Figure 3). Simultaneously for illumination, a Ti:Sapphire oscillator (Mai Tai HP, Spectra-Physics) provided continuous laser pulses of pulse duration <100 fs (λ=750 nm). A 500 M Hz oscilloscope (GDS-3504, Instek) was used to measure the pulse repetition rate (79.56 M Hz). The laser pulses were gated by electro-optical modulators, and converted to white light by a photonic crystal fiber (SCG-800, Newport) to capture diffraction-suppressed ultrafast micrographs [14]. The real time pre and post impact events were captured using a low-noise and high-quantum-yield digital camera (C11440-22C, Hamamatsu Photonics). Impact (V) and rebound (V) velocities were calculated by measuring the distance covered by the particle in the given period (images interframe time). The microparticles adhere to the target substrate after crossing the threshold velocity named as critical impact velocity. The critical velocity was also determined for each type of Cu powder (Vr=0).

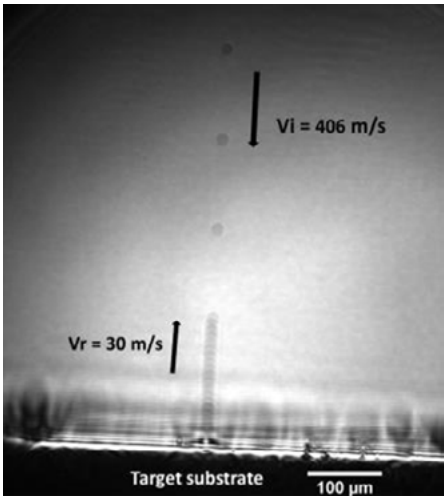

Figure 3: The collision and rebound of a Praxar Cu particle with the HP- Al target substrate.

Test Procedure

Cold spray

Cold spray samples from the first paper, "Effectiveness of Nanomaterial Copper Cold Spray Surfaces on Inactivation of Influenza A Virus" [6]. were used. The pure Cu cold spray coatings on aluminum substrates are approximately 0.05 mm thick. The nano copper (Eltron) was produced by spray drying and the conventional copper (Praxair Cu-159) through gas atomization. Due to the low mass of the nano-particles, they are bound into agglomerates using conventional Cu as the binder and spray dried [1,3,5,16,17]. For more information on the materials and cold spray process parameters see reference 1.

Laser induced projectile impact testing

Measuring the distance covered by the particle in the given period (images interframe time). The microparticles adhere to the target substrate after crossing the threshold velocity named as critical impact velocity (Figure 4). The critical velocity was also determined for each type of Cu powder (Vr=0).

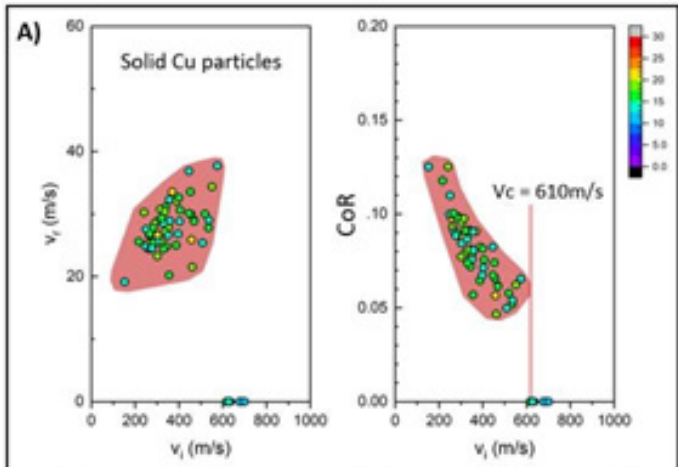

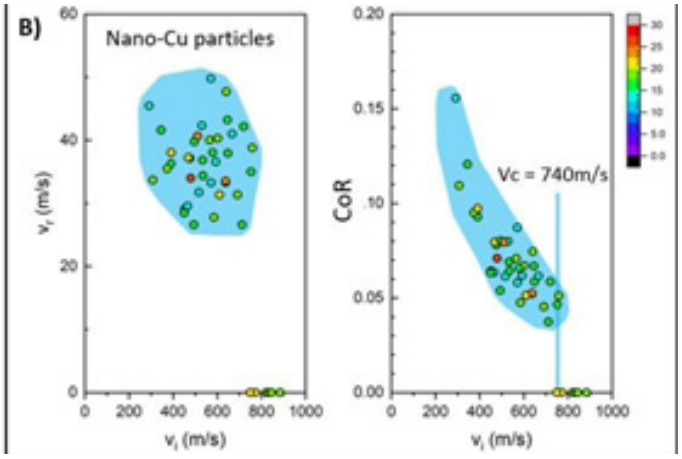

Figure 4: Rebound Velocity and COR vs. Impact Velocity for A) Conventional (Solid Cu), B) Nano-agglomerate Cu (Nano Cu) powder

Characterization: The analysis of the cross section and high-resolution SEM of the sample was performed by a Dualbeam FIB [18]. (Thermo Fisher Scientific Strata 400S). A~2 µm layer of Platinum was deposited on the surface of the sample prior to FIB. After a fine milled surface was achieved following cross sectioning, the immersionmode SEM images were taken at a tilt angle of 52°.

Microstructural and composition analysis

SEM: SEM was used to analyze the microstructure of both loose powders as well as the cold sprayed parts. Samples were mounted in metallurgical epoxy mounts, and then mechanically polished to a 0.05 µ m finish for analysis. Two orientations were studied – cross-section as well as top-down. SEM analysis was performed in a Zeiss EVO MA-10 and in the Joel JSM-7000F FE SEM at an accelerating voltage of 10 and 15 kV with both backscatter (BSE) and secondary (SE) electron detectors. Samples were then etched in 50/50 NI/DI H_2O for 15 seconds and 25/75 Ni/DI H2O for 5 seconds for conventional and nanomaterial Cu respectively and re-imaged.

EDS: EDS was performed using Bruker Nano GmbH with the Zeiss SEM for cross-sectioned powder. Oxford Instruments X-MaxN was used with the JEOL 7000 FE SEM for cross-sectioned consolidated samples. Software ran for 5 minutes prior to data collection, and dead time ranged from 2-5%. A rate of 20 kilo counts was used for the SEM and ~3000 counts per second for the FE SEM.

EBSD: EBSD analysis was performed at 25 kV in a FE-SEM (JEOL 7000F) with a NordlysMax2 detector (Oxford). Data was collected for cross-sections of powder, consolidated, and top-down polished consolidated samples (Figure 5). Step sizes used were 0.1 um and 0.316 um for nano-agglomerate and conventional Cu powder, respectively. Since the step size for the nano-agglomerate powder was so small, data was collected for only part of the grain. Consolidated nanomaterial Cu ran an area of 6 um x 4 um with a step size of 0.1 um for 1 h and 20 min. Consolidated conventional Cu ran an area of 10.5 um x 2 um with a step size of 0.1 um for 1 h 20 min, but this data was too charged and the beam was rastering empty space. Data was collected again using a 0.316 um step size for 20 min; this data is

present in the paper.

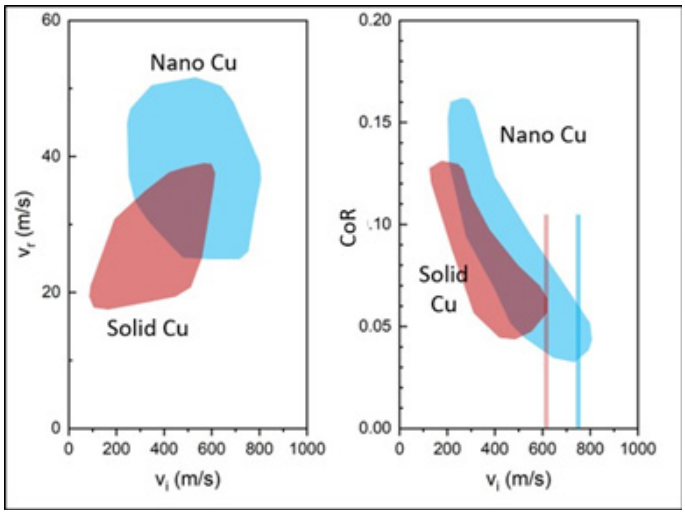

Figure 5: Rebound Velocity and COR vs. Impact Velocity for Conventional (solid Cu) and Nano-agglomerate Cu (Nano Cu) powder.

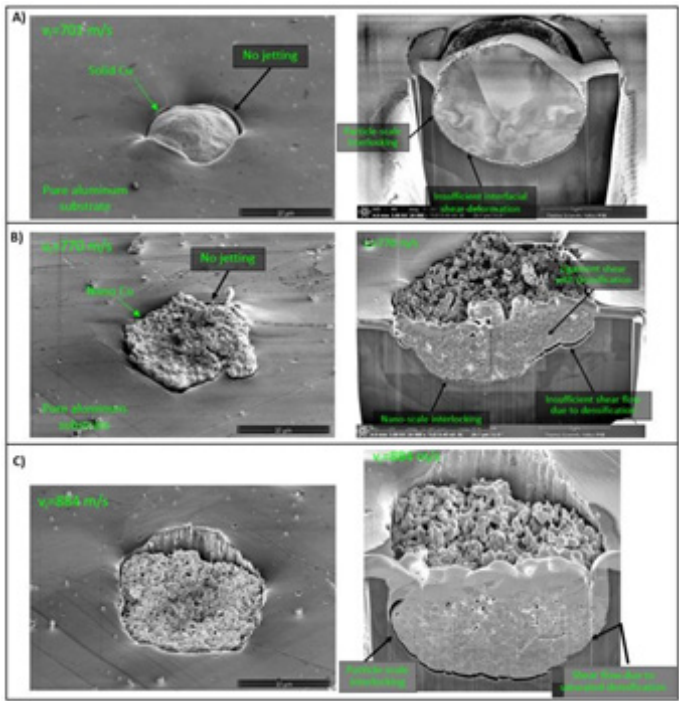

Figure 6: LIPIT of A) convnetional Cu powder particle at 701 m/s, and nano-aggomerate Cu powder particle at B) 770 m/s, C) 884 m/s.

Consolidated samples were prepped the same as for SEM, then a final polish using an Ar-ionmill at 6 kV was performed to remove any surface stresses. Powder was mounted on carbon paint on a silicon wafer and then cut down in half using a JEOL argon cross-section polisher at 6 kV for 2 hours. Mounted powder was flipped sideways in the cross-section polisher to cut powder in half (Figure 6).

XRD: WPI's PANalytical Empyrean X-ray Diffraction machine was used with a Cu tube and Ni filter from 20 to 140 2 theta at 45 KV and 40 Ma, with a ½ degree divergence slit, 1 degree anti-scatter slit, 0.04 radian soller slit, 10 mm mask, and a time per step of 10. Prior to running, the depth was checked with a goniometer and a depth of 1 was confirmed (Table 1).

Sample:	Orientation:	Hardness (G Pa): k
Nanomaterial Cu	Top-down	2.37 +/- 0.19 s
Conventional Cu	Top-down	2.01 +/- 0.04

Table 1: Nanoindentation of Consolidated Cu CS

Results were collected and analyzed using DataViewer and HighScore Plus software. Results were compared against reference PDF4 database, with PDFs 00-004-0836, 00-005-0061, 00-005-0667 for Cu, CuO, and Cu_2O, respectively.

Mechanical analysis

Static nanoindentation is performed using iMicro by Nanomechanics Inc. Consolidated top-down nanoindents are made for both conventional and nanomaterial Cu CS. A Berkovich-shaped diamond indenter tip (Micro Star Technologies) and pre-defined "Express Test for Thin Films Large Table-Batch" was used. All of the nanoindentation samples were mounted prior to testing (see section 2.3.1). 5 x 5 indent array was defined for each of the samples.

Results and Discussion

Powder microstructure

EBSD shows a difference between the conventional and nano-agglomerate powder where the latter has much finer microstructure and greater porosity. Due to the porosity of the sample, it is difficult for EBSD to provide a clear image for grain size of the nano-agglomerate powder. Percent porosity of the powder is further detailed in the pre-impact micrograph in section 3.2.

The nano-agglomerate powder grains are smaller and have more changes in orientation than the conventional Cu powder (Figure 7). For conventional Cu there is a range of powder sizes made evident by the different phase orientations, where grains range from below 1 um to above 10 um.

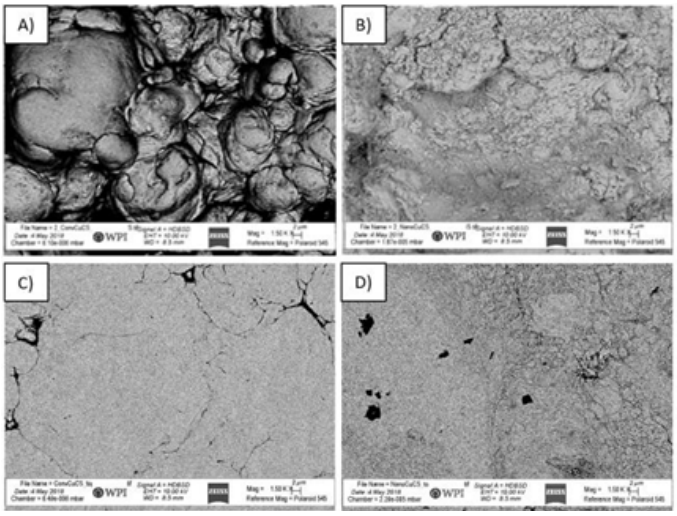

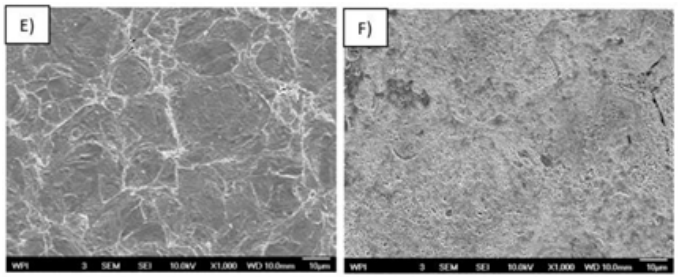

Figure 7: SEM backscatter micrograph of top-down consolidated A) conventional Cu, B) nanomaterial Cu, C) polished conventional Cu, D) polished nanomaterial Cu. FE SEM micrograph of top-down polished etched consolidated E) conventional Cu, F) nanomaterial Cu.

When looking at the etched conventional Cu powder samples, it appears that the grains are well defined in the 5-10 um range. However, based on the range of grain sizes shown in EBSD, it is possible that only the high angle grain boundaries are visible in the etched sample [19].

Laser induced projectile impact test

A pre-impact micrograph of the nano-agglomerate powder is shown in (Figure 8). The powder is fabricated by spray drying nano-agglomerates of nano Cu particles held together by a pure Cu binder. The spray drying process in combination with the use of nano particles produces significant powder porosity as compared to the gas atomization process for conventional Cu powder.

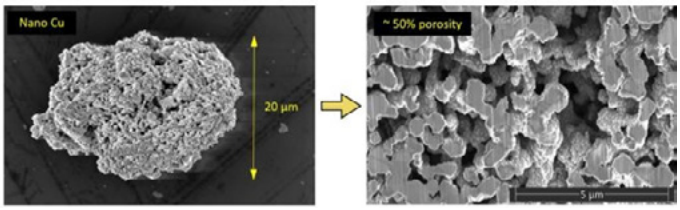

Figure 8: Micrograph of nano-agglomerate Cu powder porosity.

The impacted conventional Cu powder and nano-agglomerate powder sprayed at 701 m/s and 770 m/s respectively do not appear to have any jetting. When cross-sectioned, both have some areas at the particle-substrate interface with firm interlocking and other areas where there is a slight gap. In conventional Cu this is due to lack of shear deformation of the particle [2]. For nano-agglomerate Cu powder, the densification of the porous structure away from the substrate causes the lack of shear flow at the particle-substrate interface. There is also a distinct change in grain size and compression, with smaller grains and greater deformation at the base of the particle [9,10,20].

A change in porosity is seen in the nano-agglomerate powder as compared to the pre-impact powder. In the 884 m/s particle, there is approximately 10% porosity as compared to the 50% porosity of the particle pre-impact. With the higher velocity of 884 m/s there is also jetting present and shear flow from densification against the particle-substrate interface [21].

The nano-agglomerate Cu powder behaves similar to a foam in that energy leaves the pores on impact causing plastic deformation of the porous structures. With higher impact velocity there is greater compressive residual stress and lower porosity [4].

Overall, LIPIT shows that with increased speed there is increased particle-substrate mechanical interlocking and shear flow. Impact velocity causes vertical compression contributing to increased density and strength of the particle [19]. This is followed by lateral flow, which produces a mechanical bond between the two dissimilar metals. While physical interlocking stops the particle movement into the substrate, this does not guarantee good bond formation, as shear flow movement continues (Figure 9). Because of the shear flow that continues from pore densification in the nano-agglomerate powder, a higher critical velocity is needed to form a strong bond. Vertical impact velocity also contributes to the unique gradient microstructure, where material recrystallization from shear stress can be seen at the base of the impacted particle [MOD].

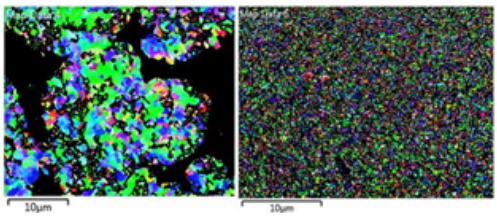

Figure 9: EBSD of polished consolidated cross-section of conventional Cu (top left) and nanomaterial Cu (top right) and top- down conventional Cu (bottom left) and nanomaterial Cu (bottom right).

Coating microstructure

Consolidated microstructure for nanomaterial and conventional Cu coatings can be seen in Figure 10. Similar to the single-splats, the consolidated coatings are highly recrystallized at the particle-substrate interface (left-side of the micrograph), followed by a middle region of deformed large particles/grains and a less deformed upper-top region (right-side) [4]. This is most noticeable in the bottom right hand micrograph of etched nanomaterial Cu.

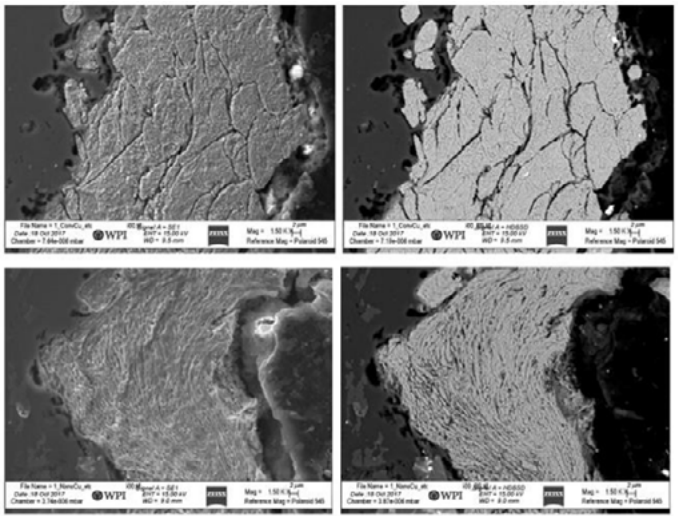

Figure 10: SEM micrographs of cross-sectioned etched consolidated conventional Cu (top), nanomaterial Cu (bottom).

The high recrystallization region is from flow stress which can

result from both temperature increase due to kinetic energy transfer on impact and from work hardening causing physical dislocation movement to form sub grains [4,9,11].

Flattened, elongated grains in the middle of the coatings show shear deformation. As the powder particles build on one another a peening effect occurs where the prior layers are work hardened and further compressed on impact. This is not as prevelant in the top-most layers of the coating [5]. In the consolidated conventional Cu, the etching is able the highlight some of the jetting and roll-ups at the particle-substrate and particle-particle interfaces [7,9].

Visually, both the EBSD top-down and cross-section micrographs show nanomaterial Cu to have a finer microstructure with much smaller grain size than that of conventional Cu. EBSD measured grain size averages for top-down conventional and nanomaterial Cu are 0.9 um and 0.43 um, respectively. EBSD measured grain size averages for the cross-sections of conventional and nanomaterial Cu are 0.57 um and 1.12 um, respectively. The top-down measurement confirms smaller grain size for the nanomaterial Cu than conventional Cu. However, the EBSD results for cross-section coatings show a discrepancy in the micrographs versus the grain-size measurement where the nanomaterial Cu appears to have smaller grain size than that of conventional Cu, but is measured as having a greater average grain size. Since the nanomaterial Cu powder is comprised of both nano particles and conventional Cu binder it is possible that the section measured with EBSD had a large amount of conventional Cu binder which skewed the results. It is also possible that EBSD is measuring the high angle-misorientation (greater than 15%) and is not accounting for low-angle-misorientation (less than 2%) [19]. this would explain why these measurements are much higher than prior values taken using TEM data [22].

TEM micrographs taken from prior work in the paper "The Effect of Nano-Scale Surface Roughness on Copper Cold Spray Inactivation of Influenza A Virus "confirm large differences in grain size for nanomaterial Cu cross-sections, showing an average range from 2.0 nm-0.1 um. Conventional Cu cross-sections were also measured with an average grain size ranging from 0.2-1.5 um [22]. These values show that a large amount of grain refinement has occurred in both samples as a result of the cold spray process [6,22].

Composition and XRD analysis

EDS data is referenced in Supplemental Section A. EDS results show Cu with some oxygen present in the powder and only Cu present for the consolidated cross-sections. Some carbon was present as well, but most likely from the mounting material.

XRD data for both powders is referenced in Supplemental Section B. XRD data supports EDS results showing peaks for Cu. Cu_2O was found to be present in the nano-agglomerate powder as well. Both powders correlated well to reference Cu PDF 00-004-0836.

For the nano-agglomerate powder, the nano particles used are amorphous (see supplemental C) and are not easily detectible by the x-rays [23]. It is likely that XRD is detecting the pure Cu binder used to bind the nano particles together and not the nano particles themselves. Further analysis (see supplemental B) of the Bragg angle and calculated d-spacing shows the same values for the powders and the reference PDF, indicating minimal contribution of strain to peak broadening [25,26]. The nano-agglomerate powder does have greater intensity than the conventional Cu powder. This may be an indicator that the Cu binder used in the nano-agglomerates is well formed and highly crystalline. It is also possible that the intensity value for conventional Cu powder is lower due to preferred orientation [23].

Mechanical data

Top-down measurements show nanomaterial Cu to have greater hardness and subsequent yeild strength as compared to conventional Cu. Hall-Petch shows an inverse relationship between hardness and grain size [13]. Based on the micrographs in Section 3.1, it is clear that nanomaterial Cu follows the Hall-Petch relation despite the presence of nano-grains. It is possible that the nanomaterial also has a greater degree of particle deformation and work hardening, both contributing factors in the increased material hardness [4].

There is a relationship between hardness and antimicrobial effectiveness [1,24]. Further analysis of the hardness and microstructure data solidifies that grain size is a major factor affecting Cu cold spray hardness and antimicrobial properties, where there is greater antimicrobial effectiveness with decreasing grain size.

Conclusions

1) Pre-impact, nano-agglomerate Cu powder has smaller grains and greater porosity then conventional Cu powder. This is due to the spray drying process and nano-particles used.

2) LIPIT shows critical velocity for 15 um sized conventional and nano-agglomerate Cu powder particles to be 610 m/s and 740 m/s, respectively. LIPIT shows that with increased velocity there is densification. Pre-impact nano-agglomerate powder porosity is 50% and post-impact it is reduced to 10%. Cross-section micrographs show gradient porosity with greater porosity at the top of the particle.

Consolidated cross-sectioned conventional and nanomaterial Cu support LIPIT results by displaying three main microstructure regions:

- Grain refined/re-crystallized area at the particle-substrate interface
- Elongated/Deformed grains in the mid-section of the particle,
- More preserved grain structure at the top of the particle.

3) All coatings have minimal to no oxides/impurities. XRD and EDS confirm Cu powder and coating composition to be pure Cu. The nano-agglomerate Cu powder did have one CuO_2 diffraction peak; however, the oxide did not appear in the consolidated coating.

4) Both cross-section and top down micrographs show nanomaterial Cu to have smaller grain size than conventional Cu. Nano indentation measurements of the surface show good

correlation between increasing hardness and decreasing grain size with hardness being much greater for nanomaterial than conventional Cu.

5) With smaller grains, nanomaterial Cu has a greater number of grain boundaries. Since Cu's antimicrobial properties are contact-based, it stands to reason that the increase in grain boundaries allows for an increase in ion flow which contributes to the more efficient contact illing of Influenza A Virus by nanomaterial Cu.

6) Additional work is needed to test LIPI on various substrates, including Cu, with different particle sizes. Work can also be done to also confirm visual findings with hardness testing of top-down and cross-sectioned impacted particles. Follow-on work is needed to confirm the hypothesized difference in ion release through corrosion testing. And efficacy testing of polished surfaces is needed to uncouple the effects of surface roughness and microstructure on antimicrobial properties of Cu cold spray.

Acknowledgement

Thank you to UMass Department of Mechanical and Industrial Engineering for Laser Induced Projectile Impact Testing.

References

1. Sundberg K., Champagne V, McNally B, Helfritch B, Sisson R (2015) Effectiveness of nanomaterial copper cold spray surfaces on inactivation of influenza a virus. J Biotechnol Biomater 5: 4.
2. Grujicic M (2003) Computional analysis of the interfacial bonding between feed-powder particles and the substrate in the cold-gas dynamic-spray process. Appl Surf Sci 219: 211-227.
3. Schmidt T (2006) Development of a generalized parameter window for cold spray deposition. Acta Mater 54: 729-742.
4. Viscusi A, (2018) A perspective review on the bonding mechanisms in cold gas dynamic spray. Surface Engineering 35: 743-771.
5. Rokni M (2017) Review of relationship between particle deformation-coating microstruture and properties in high pressure cold spray. J Therm Spray Technol 26: 1308-1355.
6. Borches C, Gartner F, Stoltenhoff T (2003) Microstructural and macroscopic properties of cold sprayed copper coatings. J Appl Phys 93: 10064-10070.
7. Sundberg K, Sousa B, Schreiber J, Walde C, Sisson R, et al. (2018) Modeling copper cold spray single-particle impact for optimized antimicrobial coatings. Appl Mater
8. Kim KH, Watanabe M, Karakita J, Kuroda S (2008) Grain refinement in a single titanium powder particle impacted at high velocity. Scr Mater 59: 768-771.
9. Lee C, Kim J (2015) Microstructure of kinetic spray coatings: A review. J Therm Spray Technol 24: 592-610.
10. Lee J, Loya P, Lou J, Thomas E (2014) Dynamic mechanical behavior of multilayer graphene via supersonic projectile penetration. Science 346: 1092-1096.
11. Villafuerte J (2015) Modern cold spray: Materials, processes, applications.
12. Callister W, Rethwisch D (2018) Materials science and engineering: An introduction, enhanced. Wiley
13. Hansen N (2004) Hall-petch relation and boundary strengthening. Scr Mater 51: 801-806.
14. Xie W, Alizadeh A, Chen Q, Champagne V, Wang X, et al. (2017) Dynamics and extreme plasticity of metallic microparticles in supersonic collisions. Scientific Reports 7: 1.
15. Chen Q, Alizadeh A, Xie W, Wang X., Champagne V, et al. (2018) High- strain-rate material behavior and adiabatic material instability in impact of micron-scale al-6061 particles. J Therm Spray Technol 27: 641-653.
16. Praxair: surface technologies. Powder Solutions: product brochure. www.praxairsurfacetechnologies.com.
17. Rolfe S (2014) email conversation and Phase I SBIR Final Report, "Advanced Nanostructured Powders for Cold Spray Applications", Eltron Research and Development Inc., 4600 Naytilus Court South Boulder, C0 80301-3241
18. Lee J, Veysset D, Singer J, Retsch M, Saini G, et al. (2012) High strain rate deformation of layered nanocomposites. N Comms 3: 1
19. Young K (2017) Microstructure and Room Temperature Compressive Deformation Behavior of Cold- Sprayed High-Strength Cu Bulk Material. J Therm Spray Technol 26: 1498-1508.
20. King P (2009) An experimental and finite element study of cold spray copper impact onto two aluminum substrates. J Therm Spray Technol 19: 629-634.
21. Fukumoto M (2009) Deposition of copper fine particles by cold spray process. Mater trans 50: 1482-1488.
22. Sundberg K, Gleason M, Haddad B, Champagne V, Brown C, et al. (2019) The effect of nano-scale surface roughness on copper cold spray inactivation of influenza a virus. Int J Nano Med & Eng 4: 33-40
23. Cullity B, Stock S (2001) Elements of x-ray diffraction. Third edition.
24. Champagne V, Helfritch, D (2013) A demonstration of the antimicrobial effectiveness of various copper surfaces. J Biol Eng 7: 8
25. Hassani M, Veysset D, Nelson K, Schuh C (2018) In-situ observations of single micro-particle impact bonding. Scr Mater 145: 9-13.
26. Theivasanthi T, Alagar M (2010) X-ray diffraction studies of copper nanopowder. Applied Physics Research 1: 112-117.